Energy Conversion and Management 103 (2015) 674–680

Contents lists available at ScienceDirect

Energy Conversion and Management

journal homepage: www.elsevier.com/locate/enconman

Heat shrink formation of a corrugated thin film thermoelectric generator

Tianlei Sun [a], Jennifer L. Peavey [b], M. David Shelby [b], Scott Ferguson [a], Brendan T. O'Connor [a,*]

[a] North Carolina State University, Department of Mechanical and Aerospace Engineering, 911 Oval Dr., Raleigh, NC 27695, United States
[b] Eastman Chemical Company, PO Box 431, Kingsport, TN 37662-0431, United States

ARTICLE INFO

Article history:
Received 28 April 2015
Accepted 5 July 2015
Available online 16 July 2015

Keywords:
Thermoelectric generator
Thin film
In-plane heat transfer
Corrugated architecture

ABSTRACT

A thin film thermoelectric (TE) generator with a corrugated architecture is demonstrated formed using a heat-shrink fabrication approach. Fabrication of the corrugated TE structure consists of depositing thin film thermoelectric elements onto a planar non-shrink polyimide substrate that is then sandwiched between two uniaxial stretch-oriented co-polyester (PET) films. The heat shrink PET films are adhered to the polyimide in select locations, such that when the structure is placed in a high temperature environment, the outer films shrink resulting in a corrugated core film and thermoelectric elements spanning between the outer PET films. The module has a cross-plane heat transfer architecture similar to a conventional bulk TE module, but with heat transfer in the plane of the thin film thermoelectric elements, which assists in maintaining a significant temperature difference across the thermoelectric junctions. In this demonstration, Ag and Ni films are used as the thermoelectric elements and a Seebeck coefficient of 14 $\mu V\ K^{-1}$ is measured with a maximum power output of 0.22 nW per couple at a temperature difference of 7.0 K. We then theoretically consider the performance of this device architecture with high performance thermoelectric materials in the heat sink limited regime. The results show that the heat-shrink approach is a simple fabrication method that may be advantageous in large-area, low power density applications. The fabrication method is also compatible with simple geometric modification to achieve various form factors and power densities to customize the TE generator for a range of applications.

1. Introduction

The direct conversion of thermal energy to electrical power without moving parts makes thermoelectric generators (TEG) a highly attractive energy conversion technology. These devices also have the advantage of having a small volume, and the ability to convert energy over a broad temperature range. However, to date there has been limited commercial adoption of TEGs due to high module costs and relative poor efficiency compared to other technologies. Recently, significant efforts have focused on developing thermoelectric (TE) materials with increased efficiency through improving the TE element's dimensionless figure of merit, $ZT = S^2\sigma T\kappa^{-1}$, where S, σ, T and κ are the Seebeck coefficient, electrical conductivity, absolute temperature, and thermal conductivity, respectively [1]. The ZT value provides an upper limit on TE power conversion efficiency and is thus a key optimization parameter [2]. Currently, there have been numerous demonstrations of thermoelectric materials with ZT values greater than 2 [3,4]. However, TEGs based on these materials will struggle to become cost effective [5]. Alternatively, low-cost thermoelectric materials based on organic and organic–inorganic hybrid systems are being developed that have recently shown promising cost-performance metrics [5,6]. Conjugated polymers have been developed with ZT as high as 0.4 [7], and hybrid solution processed materials have been shown to have ZT values as high as 0.1 [8].

While improving ZT is critical for cost competitiveness, other aspects of TEG design must also be considered to ensure low cost and high performance systems [9,10]. In particular, it is highly advantageous to develop TEG modules that are compatible with low-cost processing methods and to develop modules that do not have elaborate heat sink demands [11]. Low-cost TE processing has focused on thin-film materials that are compatible with roll-to-roll processing [12–14]. For these thin-film elements, heat transfer across the plane of the film (cross-plane TEs) is the most common module architecture [15,16]. However, maintaining a large temperature difference across the thin film junctions (and thus increasing power output) becomes a challenge [11]. Thin film TEGs can also be designed such that heat transfer occurs in the plane of the film (in-plane TEs) [17–19]. However, this design is

* Corresponding author.
E-mail address: btoconno@ncsu.edu (B.T. O'Connor).

http://dx.doi.org/10.1016/j.enconman.2015.07.016
0196-8904/

Nomenclature

A_m	project area of the thermoelectric module
A_S	summed cross section area of polyimide substrate
A_{TE}	summed cross section area of the thermoelectric couples
G	overall thermal conductance of the thermoelectric elements and substrate
h	heat transfer coefficient
h'	modified heat transfer coefficient
I	electric current
L	leg length
n	number of thermoelectric couples
P	total output power
p_{max}	maximum power density
R_i	thermoelectric internal electric resistance
R_L	load electrical resistance
R_{spr}	heat spreading thermal resistance
S	seebeck coefficient
S_{pn}	seebeck coefficient of one thermoelectric couple
T	absolute temperature
T_g	glass transition temperature
t_{TE}	thickness of the thermoelectric elements
w	width of thermoelectric elements
ZT	thermoelectric figure of merit

Greek symbols

α	stacking angle
Δ	change in a property
κ	thermal conductivity
ρ	electrical resistivity
σ	electrical conductivity

Subscripts

C	cold side
F	ambient environment
H	hot side
max	maximum
opt	optimal
s	substrate
TE	thermoelectric element

not compatible with large area heat sources, and thus not typically applied for power generation [20]. An alternative thin-film thermoelectric design is to place the thin film thermoelectric elements in a corrugated arrangement between thermal interface planes, as illustrated in Fig. 1 and labeled here as a corrugated TE generator (C-TEG). In this design, heat transfer is in the plane of the thin-film thermoelectric elements, effectively increasing the TE element leg-length and improving the ability to maintain a finite temperature difference across the thermoelectric junctions. While heat transfer is in the plane of the thin film, the module remains a cross-plane TE design making it compatible with large area applications.

There have been several previous demonstrations of similar corrugated-type TEGs [19,21–23]. In these demonstrations, there have been two primary methods of fabrication. In the first approach, the TE elements are deposited onto a flat plastic substrate, the substrate is then adhered to a secondary corrugated surface [22]. The secondary surface holds the thin film in the corrugated shape and acts to separate the cold and hot side junctions. In this approach, the secondary element is a solid material that will result in a significant reduction in temperature difference across the thermocouples lowering power generation and efficiency. The second approach consists of using a thin film plastic substrate that is held in a sinusoidal mold. The thermoelectric elements are vacuum deposited onto the substrate and then the plastic substrate is removed from the mold and bonded to planar plastic plates to maintain the corrugated module architecture. This is an effective approach to form the corrugated module, however depositing onto a non-planar substrate is a challenge and requires vapor deposition methods that are unable to take advantage of low-cost solution processing methods of organic and hybrid materials [21].

Here, we further demonstrate a method of fabricating a C-TEG by using an innovative plastic heat shrink approach [24]. This method is compatible with processing thermoelectric elements onto flat surfaces that are then formed into the C-TEG geometry. This approach has the advantage of simple corrugated element formation that results in freestanding thermoelectric legs that will minimize parasitic thermal losses. The experimental performance of a thermally formed C-TEG with metallic thermoelectric elements is characterized in detail and compared to finite element and analytical models. To consider the opportunities of this device architecture, it is investigated theoretically with high performance thermoelectric materials and the architecture is optimized using thermal impedance analysis.

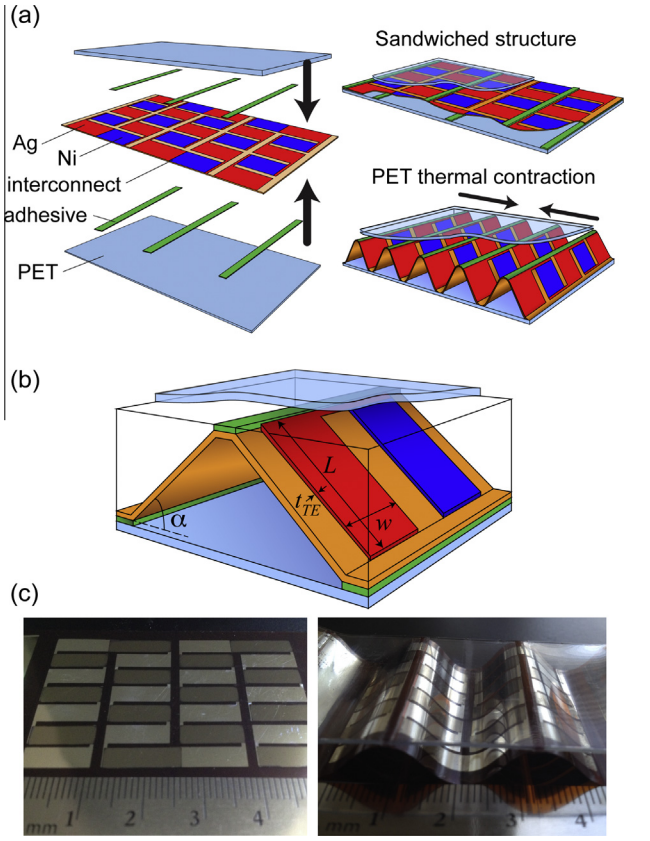

Fig. 1. (a) Schematic illustration of the fabrication process for the corrugated TEG device, including the stack of heat-shrink PET, adhesives, and thermoelectric couples on a polyimide substrate. The layers are all combined forming a sandwiched structure that is then thermally formed into the corrugated TEG. (b) Simplified geometric model of corrugated TEG device, with thermoelectric leg dimensions including thermoelectric thickness (t_{TE}), length (L), width (w), and stacking angle (α). (c) Photos of the corrugated TEG device before and after being thermally formed.

2. Corrugated thermoelectric module fabrication

A schematic of the fabrication process, and final structure is illustrated in Fig. 1(a). For proof-of-concept purposes, the thermoelectric elements consisted of Ag and Ni thin films deposited by vacuum thermal evaporation onto a 130-μm thick polyimide substrate, and patterned using a shadow mask. The polyimide film was the core layer of the TEG module and the support for the thin-film thermoelectric legs. The thermoelectric elements were 140-nm thick, 4-mm wide and variable in length. The thermoelectric legs were electrically connected laterally in a row and then between rows at the last TE elements with Ag thin films, as illustrated in Fig. 1(a) and pictured in Fig. 1(c). There was approximately 0.5 mm overlap of the metallic elements to form the electrical junctions. The non-shrink polyimide core was then attached to heat-shrink polyester (PET) films on each side of the polyimide with polymer adhesive placed between the rows of the thermocouples in alternating fashion. The outer layers were uniaxial stretch-oriented having a glass transition temperature (T_g) of approximately 345 K. The outer layers were extruded to create the un-oriented base material and then uniaxially stretched at a temperature of approximately 355 K [24]. The three layer planar composite structure was then placed in a vacuum oven at 383 K causing the PET sheets to shrink and forcing the polyimide interlayer to form and maintain a sinusoidal shape. In this demonstration, 630-μm thick PET films were stretched by 33%, resulting in films with a shrink of approximately 25% after heating. An example of the fabricated hybrid TEG is pictured in Fig. 1(c) and is composed of three and a half Ag-Ni couples per row with legs that are 12 mm long and 4 mm wide. Note that Ag and Ni were chosen for their good thermoelectric properties among metals. These materials are also ductile and adhere well to the polyimide allowing for bending during TEG formation without mechanical failure.

3. Results and discussion

3.1. Performance analysis

The performance of the TE couples was characterized prior to the attachment of the PET outer layers, and then again after the completed corrugated TE fabrication process as described above. The TE couples tested prior to device fabrication were in a planar configuration. The temperature difference was achieved using commercial thermoelectric modules, one on each side of the couples with one heating and the other cooling. The planar TE device was placed across the commercial thermoelectric modules. The temperature at the junctions of the test structure was measured with a surface thermocouple (Model 88014, Omega Engineering) placed in close proximity to the metal junctions. For the C-TEG testing, the commercial thermoelectric modules were placed on each side of the test module. Again, one module was set to cool and the other to heat to generate a temperature difference across the module. In this case a thermocouple (5-SRTC, Omega Engineering) was adhered at the metal junctions using thermal paste. The current–voltage characteristics of the test devices were measured using a semiconductor parameter analyzer (HP 4156b). In Fig. 2(a) the open circuit voltage is given as a function of temperature difference between the thermocouple junctions (ΔT) for a row of 3 couples and a row of 10 couples with 8-mm long legs. From the slope of the curve the Seebeck coefficient of one couple (S_{pn}) is found to be 19.0 μV K^{-1} for the 3 TE couples in the flat sheet configuration, which matches well to previous experimental result of 19.2 μV K^{-1} [24]. However, S_{pn} drops down to 14.2 μV K^{-1} when formed into the C-TEG design. Similarly, the electrical resistivity was found to be 368 nΩ m while flat and 875 nΩ m when bent. This resistivity is higher than typically observed for these metals in bulk form (20 nΩ m and 190 nΩ m for Ag and Ni, respectively) [26–28]. The large resistivity of the films in the flat configuration is attributed to the vacuum deposition process and thin film nature, which has previously been shown to increase the resistivity of metals compared to their bulk counterpart [29,30]. The change in properties when forming the C-TEG module is likely due to an increase in dislocation density and other defects associated with the bending process. The smallest radius of curvature observed for the thermoelectric couples with leg length of 8 mm was found to be approximately 3.8 mm. Previous research considering the change in conductivity of thin metal films with bending radius showed similar changes in electrical resistivity [31]. Critically, the metallic interconnection of the thermoelectric legs for different rows, pictured in Fig. 1(c), will see the smallest radius of curvature

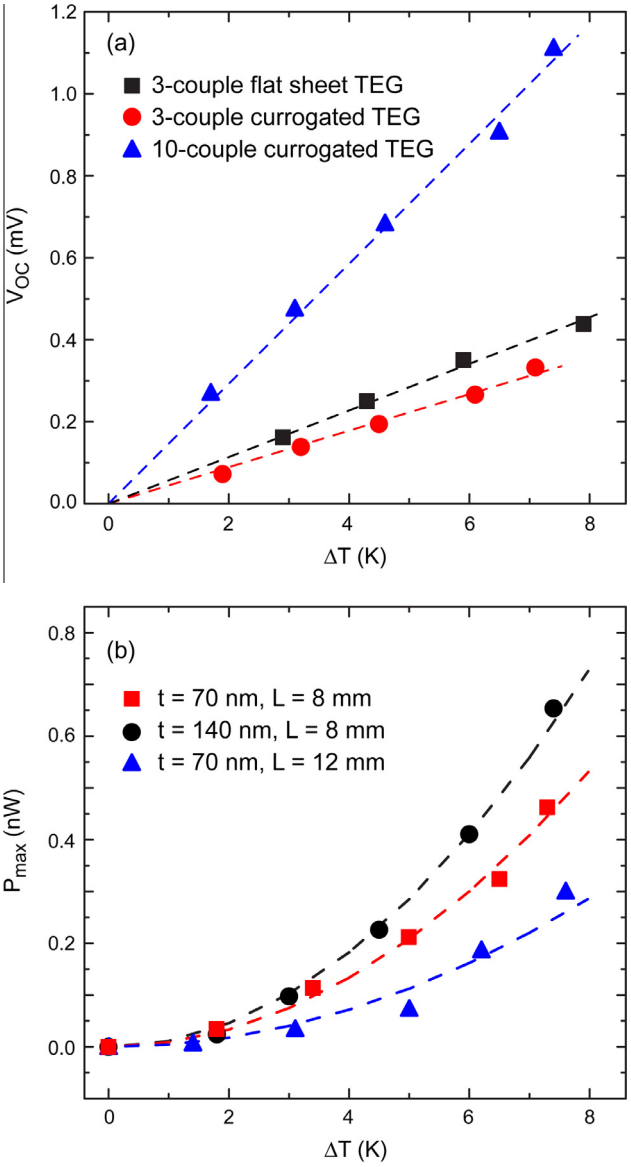

Fig. 2. (a) Open circuit voltage (V_{oc}) as a function of the temperature difference across the couples (ΔT) for various thermocouple configurations, 3 TE couples in a flat sheet, 3 TE couples in the corrugated structure, and 10 TE couples in the corrugated structure. The linear fits to the data are used to determine the average Seebeck coefficient of the thermoelectric couple. (b) The maximum power output for different geometries of the thermoelectric thin film material in the corrugated structure for 3 thermocouples. The line fit to the experimental data is made using Eq. (2).

and the metal film will be in contact with the polymer adhesive. To determine if this has a large impact on performance, the Seebeck coefficient was measured across 10 thermocouples over multiple rows, which includes the interconnecting Ag film between rows. The average S_{pn} was found to be 14.0 μV K^{-1} per couple, showing negligible performance loss associated with this interconnection.

The output voltage and output power for 3 TE couples in one row of the C-TEG was investigated experimentally and with finite element numerical simulation using ANSYS [32], for a ΔT of 7.0 K. The finite element model consisted of 598,225 nodes and 295,719 elements using an auto-generated mesh. The model assumes planar legs as illustrated in Fig. 1(b). The difference in the finite element model output using sinusoidal legs and the straight leg approximation has previously been shown to be negligible [33]. Experimentally, the maximum output power was found to be approximately 0.67 nW at a current of 4.1 μA, as shown in Fig. 3. The result from the finite element simulation matches well with the experimental measurement, with a maximum output power of 0.65 nW. Generally, the total output power (P) of TEGs can be given by [11],

$$P = \frac{(nS_{pn}\Delta T)^2 R_L}{(R_i + R_L)^2}, \tag{1}$$

where n is the number of the TE couples, R_i is the TEG internal electrical resistance and R_L is the load electrical resistance. The maximum output power occurs when the load electrical resistance is equal to the internal electrical resistance of TEG resulting in,

$$P_{max} = \frac{(nS_{pn}\Delta T)^2}{4R_i}. \tag{2}$$

The geometry of the TE couples directly impacts the maximum output power due to R_i given by,

$$R_i = \frac{\rho L}{w t_{TE}}, \tag{3}$$

where ρ is the combined electrical resistivity, L is the leg length, w is width of TE elements and t_{TE} is thickness of the elements. The experimental maximum output power with variation in temperature difference for various L/t_{TE} ratios is given in Fig. 2(b) and is compared to the predicted power from Eq. (2). It is found that P_{max} increases with ΔT following a parabolic relationship as expected. It is clear that the thicker film and shorter leg length result in high power output following the relationship that power density is proportional to $(wt_{TE})/L$, as given by Eq. (2) [34].

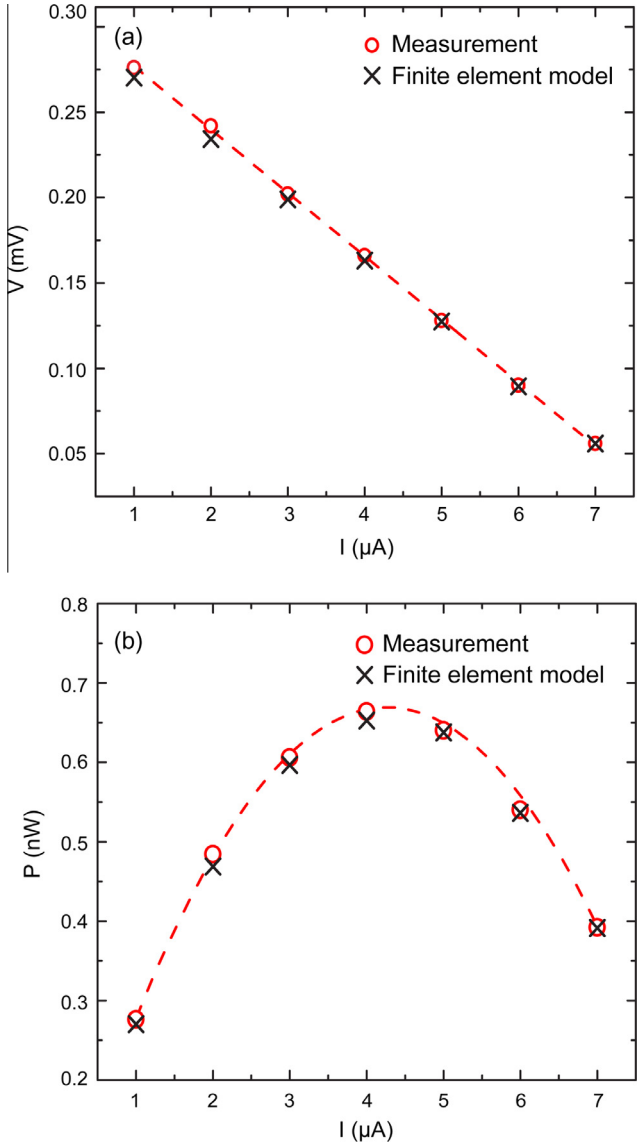

Fig. 3. (a) Voltage output (V) and (b) power output (P) of 3-couples of the C-TEG as function of current (I) for a temperature difference across the couples (ΔT) of 7.0 K. The measurement is compared to numerical finite element simulations.

3.2. Theoretical performance optimization

The geometry of the experimentally demonstrated modules was selected based on availability of pre-stretched PET, stability of the thermally formed corrugated film, and ability to easily probe the temperature profile across the thermocouples. However, the resulting modules may not be the optimal geometry for power generation. Similarly, high performance materials may be employed as long as bending during fabrication does not significantly impact their properties. With this in mind, a dimensional and material analysis is theoretically conducted on the C-TEG design to consider the performance potential of this architecture. With the goal of minimizing the system cost, it is expected that the module will operate in the heat sink limited regime [9,11]. The TEG is heat sink limited when the output power of the system is limited by the ability to transfer heat to or away from the thermoelectric couples. This would be expected for a TEG system without elaborate heat sink designs. Here, the TEG performance is optimized under the conditions of a constant hot side temperature of the thermoelectric couple (T_H), and heat rejection being limited by natural convection [9,11]. Optimal performance of this system is found under thermal impedance matching conditions. Details of this approach have been previously described [9,11]. Here, we provide a brief review of the analysis method. In thermoelectric operation, the convective heat transfer from the cold side of the module is equivalent to the summed conduction through the module, Peltier heat transfer, and joule heating, given by,

$$hA_m(T_C - T_F) = G(T_H - T_C) + S_{pn}T_C I + \frac{1}{2}I^2 R_i, \tag{4}$$

where h is the heat transfer coefficient, A_m is the projected area of the TEG module, T_C is the cold side temperature of the TE couple, T_F is the environment temperature, I is electric current, and G is overall thermal conductance of the TE elements and substrate given by,

$$G = \frac{\kappa_{TE}A_{TE}}{L} + \frac{\kappa_s A_s}{L}, \tag{5}$$

where κ_{TE} is the thermal conductivity of the TE element, A_{TE} is the summed cross section area of the TE couples, κ_s is the thermal

conductivity of the polyimide substrate and A_s is the summed cross section area of the polyimide substrate. To simplify the calculation, Peltier heat transfer and joule heating, which are relatively small compared with heat conduction are neglected [11] resulting in,

$$hA_m(T_C - T_F) \approx G(T_H - T_C). \quad (6)$$

The design of the C-TEG module will typically result in a low areal packing density of thermoelectric elements as compared to a conventional bulk TEG. This requires that the thermal resistance caused by heat spreading also be included in the optimization. Heat spreading occurs when heat flows through materials that have a change in cross-sectional area [35], which in our case happens when heat flows between the outer PET films and the thermoelectric legs. The thermal resistance associated with heat spreading can be accounted for by modifying the heat transfer coefficient h resulting in a modified heat transfer coefficient h' given by [11,35,36],

$$h' = \frac{1}{A_m R_{spr} + 1/h}, \quad (7)$$

where R_{spr} is the heat spreading resistance. One important factor affecting R_{spr} is thermal conductivity of the outer layer material, which in our case is PET [35]. Applying a high thermal conductivity material will dramatically decrease the heat spreading capacity and thus increase the overall power density. A possible approach is to coat a metal layer on the exterior of the PET layer to minimize heat spreading resistance. Combining Eqs. (2), (6) and (7), the maximum power density (p_{max}) is given as,

$$p_{max} = \frac{h'^2 A_m (T_H - T_F)^2 S_{pn}^2 A_{TE}}{4(h'A_m + G)^2 L\rho}. \quad (8)$$

In this analysis, T_H = 302 K, T_F = 295 K, and h = 5 W m^{-2} K^{-1}. The heat transfer coefficient represents natural convection of a vertical plate in air with a modest temperature difference between T_C and T_F [37].

Based on this analysis, we consider p_{max} with a variation in L and α for the Ag–Ni elements with experimentally determined materials properties, with results given in Fig. 4. It is important to note that conduction through the air cavity within the TE module is considered negligible in this analysis. This is a common assumption that does not typically have a large impact on performance. However, at small values of α, conduction through the cavity may become a significant factor and caution in the accuracy of this assumption is warranted. Here, we find that for a constant L, p_{max} increases as α becomes larger as a result of the increase in thermoelectric element packing density (i.e. increased fill factor). If α is held constant, there exists an optimal leg length (L_{opt}) that results in p_{max}. In the experimental conditions, α was approximately 41°, which would result in L_{opt} to be approximately 3 mm. For verification of the model, the experimental results with the same boundary conditions (T_H = 302 K, T_F = 295 K, h = 5 W m^{-2} K^{-1}) are also plotted in Fig. 4, and are shown to matched well with the calculated data. Differences between the model and experimental results may be associated with unaccounted for geometric variations, thermal contact resistances, and heat transfer coefficient.

Thermoelectric materials with higher ZT should significantly improve the power generation of the C-TEG module. To consider the performance opportunity of the C-TEG design with advanced materials, we theoretically consider the performance with high performance Bi_2Te_3 based elements. In this case we use S_{pn} = 236 μV K^{-1}, ρ = 12.3 μΩ m, κ = 0.57 W m^{-1} K^{-1}, resulting in a ZT value of approximately 2.38 at room temperature, similar to previous demonstrations [3]. While the thin film thermoelectric elements should aid flexibility, the Bi_2Te_3 elements may not necessarily have the ability to flex during processing without fracture [38]. Nevertheless, the material is chosen to represent a realistic, high performance system that may be achieved with more compliant materials in the near future [7,20]. The power density of the module is given in Fig. 5(a) with variation in L and α, with t_{TE} held constant at 75 μm, and in Fig. 5(b) for a variation in t_{TE} and L, with α held constant at 68° (which represents a shrink ratio of approximately 50%, in-place of the experimentally demonstrated 20%). The larger α will increase the power density of the module, and the value chosen is based on a realistically achievable shrink ratio for drawn polymer films. A similar trend is found for p_{max} with variation in α and L as observed with the metal TE elements. In Fig. 5(b), it is observed that the thickness of the thermoelectric elements increases the power out of the device but L_{opt} is found to be relatively constant. Due to the heat sink limited regime, at high α, L_{opt} is found to be larger than observed in the analysis of the metal TE couples resulting in greater compatibility with simple scalable processing. According to Mayer and Ram [11], an excessively high packing density will result in reduced performance due to heat sink limitations. However, performance loss associated with excessive packing density is not observed in Fig. 5. This is due to the packing limits inherent with the C-TEG design. The thermal conductance of the TE element is very small due to the small thickness and long leg length, and the fill factor remains low even when α is equal to 90° due to the spacing associated with the polyimide substrate (~0.12 mm) and adhesive (~2 mm). The substrate thickness will also have an effect on the power density p_{max} by increasing parasitic heat transfer with increasing thickness. The impact of substrate thickness has previously been investigated for a corrugated TE cooler [33]. It was found that the losses can be relatively low for moderate temperature differences across the module [33].

Finally, for comparison, a conventional bulk thermoelectric (B-TEG) module with the same areal density of thermoelectric material (kg m^{-2}) as the C-TEG under the same boundary conditions is considered. Here the B-TEG is considered with high thermal conductivity ceramic interface plates (κ = 150 W m^{-1} K^{-1}), and TE elements without a substrate support. For a C-TEG with t_{TE} = 75 μm and α = 68°, L_{opt} is found to be 4 mm resulting in

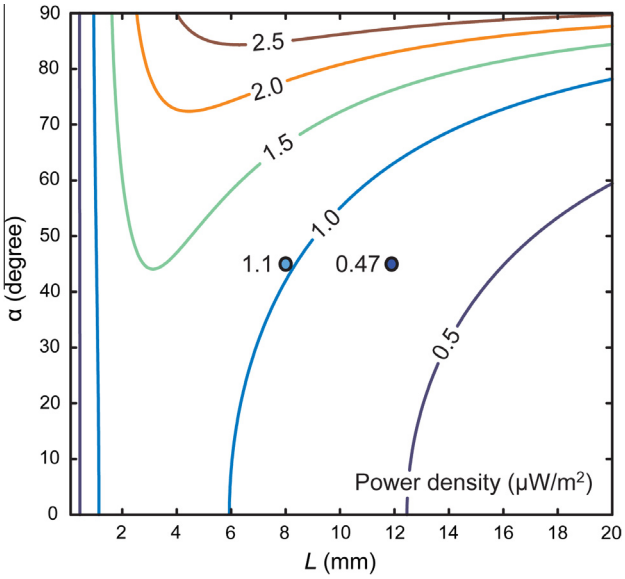

Fig. 4. The theoretical maximum power density (p_{max}) of a C-TEG module as a function of the thermoelectric couple leg length and leg angle (α) when employing the Ag-Ni couples under the heat sink limited conditions. Experimental maximum power density under the same boundary conditions for the fabricated devices is also provided (dots).

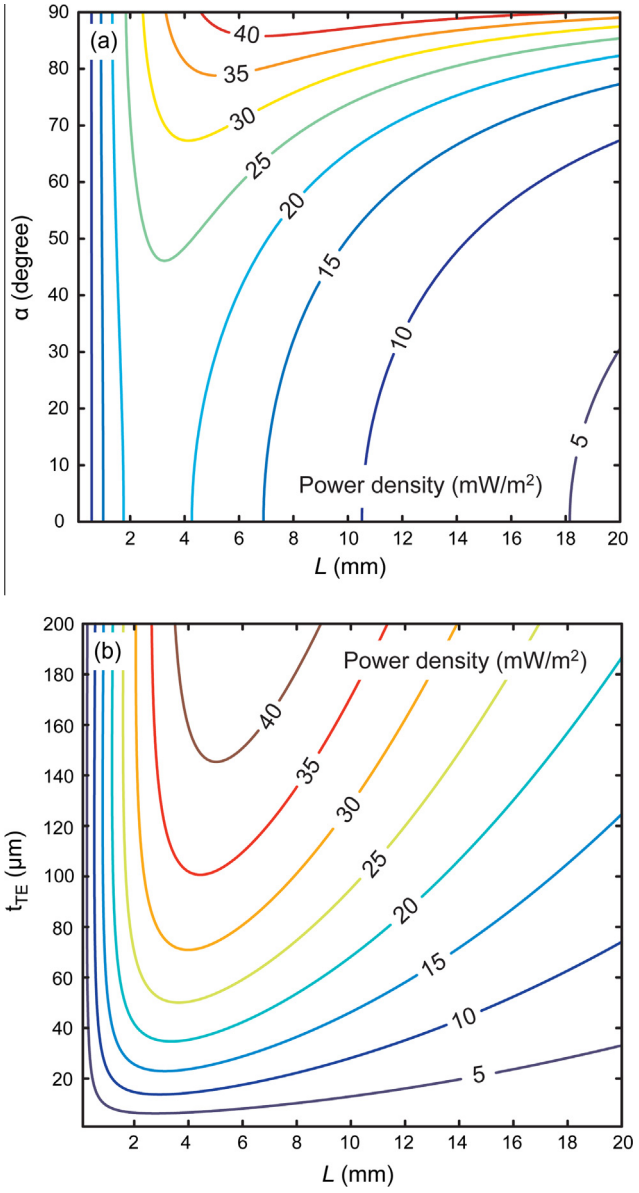

Fig. 5. Geometric analysis of the maximum power density for a C-TEG based on Bi_2Te_3 thermoelectric couples. (a) Power density as a function of leg length and leg stacking angle for a constant thermoelectric element thickness (t_{TE}) of 75 μm. (b) Power density as a function of leg length and t_{TE} for a C-TEG with a constant leg stacking angle (α) of 68°.

0.3 kg m^{-2} of Bi_2Te_3 and p_{max} = 31 mW m^{-2}. Using a comparable areal density of TE material, the B-TEG will have a maximum power density of 83 mW m^{-2}. The difference mainly comes from the application of the high thermal conductivity interface plates on the B-TEG. Improving the thermal conductivity of the PET layer in the C-TEG with metal coatings or through embedded high conductivity particles will improve module performance and minimize any differences in performance. This suggests that the C-TEG can have performance comparable to B-TEG modules for similar thermoelectric element densities.

4. Conclusion

In this paper, we experimentally demonstrated an innovative thermally formed thermoelectric device that employs thin film thermoelectric elements supported on a plastic substrate that are oriented in a corrugated fashion to resemble a convention bulk thermoelectric architecture. The demonstrated Ag-Ni thermoelectric based devices were found to have a maximum output power of approximately 0.22 nW per couple when under a 7.0 K temperature difference. While there is slight performance degradation due to the processing approach, the performance is similar to other demonstrations of Ag-Ni thermocouples [25]. We then theoretically consider the performance of this system under a heat sink limited operating regime, finding that an optimal thermoelectric leg length between 3 and 4 mm occurs over a wide range of leg stacking angles, and an optimal power output of 1.5 μW m^{-2} is found for a stacking angle similar to that experimentally demonstrated (α = 40°). The theoretical results are then extrapolated to high performance thermoelectric materials showing that for a realistic shrink ratio of 50%, a power density of 31 mW m^{-2} can be achieved. This power output is similar to a bulk thermoelectric module for a comparable areal density of thermoelectric material. Further increases in performance are expected with implementation of thermal interface layers with higher thermal conductivity.

The results suggest that for low power density applications with low-quality waste heat, the heat shrink C-TEG module may provide a cost-performance advantage as compared to conventional TEs. This is due in-part to the simple heat-shrink approach that is compatible with low-cost, scalable fabrication methods. The geometric details of the C-TEG module can also be easily modified by varying the heat shrink ratio of the individual PET layers. This includes the formation of cylindrical shapes [24]. This allows for application to non-planar geometries with the ability to optimize element packing density for a specific application.

Acknowledgement

The authors gratefully thank Eastman Chemical Company for financial support of this work.

References

[1] Rowe D. CRC Handbook of Thermoelectrics. 1st ed. CRC Press; 1995.
[2] Chen G, Dresselhaus MS, Dresselhaus G, Fleurial J-P, Caillat T. Recent developments in thermoelectric materials. Int Mater Rev 2003;48:45.
[3] Venkatasubramanian R, Siivola E, Colpitts T, O'Quinn B. Thin-film thermoelectric devices with high room-temperature figures of merit. Nature 2001;413:597.
[4] Shakouri A. Recent developments in semiconductor thermoelectric physics and materials. Annu Rev Mater Res 2011;41:399.
[5] LeBlanc S, Yee SK, Scullin ML, Dames C, Goodson KE. Material and manufacturing cost considerations for thermoelectrics. Renew Sustain Energy Rev 2014;32:313.
[6] Malen JA, Yee SK, Majumdar A, Segalman RA. Fundamentals of energy transport, energy conversion, and thermal properties in organic-inorganic heterojunctions. Chem Phys Lett 2010;491:109.
[7] Kim G-H, Shao L, Zhang K, Pipe KP. Engineered doping of organic semiconductors for enhanced thermoelectric efficiency. Nat Mater 2013;12:719.
[8] See KC, Feser JP, Chen CE, Majumdar A, Urban JJ, Segalman RA. Water-processable polymer–nanocrystal hybrids for thermoelectrics. Nano Lett 2010;10:4664.
[9] Yazawa K, Shakouri A. Cost-efficiency trade-off and the design of thermoelectric power generators. Environ Sci Technol 2011;45:7548.
[10] Kim R, Datta S, Lundstrom MS. Influence of dimensionality on thermoelectric device performance. J Appl Phys 2009;105:034506.
[11] Mayer PM, Ram RJ. Optimization of heat sink-limited thermoelectric generators. Nanoscale Microscale Thermophys Eng 2006;10:143.
[12] Navone C, Soulier M, Plissonnier M, Seiler AL. Development of (Bi, Sb)2(Te, Se)3-based thermoelectric modules by a screen-printing process. J Electron Mater 2010;39:1755.
[13] Kim SJ, We JH, Kim JS, Kim GS, Cho BJ. Thermoelectric properties of P-type Sb_2Te_3 thick film processed by a screen-printing technique and a subsequent annealing process. J Alloys Compd 2014;582:177.
[14] We JH, Kim SJ, Kim GS, Cho BJ. Improvement of thermoelectric properties of screen-printed Bi_2Te_3 thick film by optimization of the annealing process. J Alloys Compd 2013;552:107.

[15] Lee H-B, Yang HJ, We JH, Kim K, Choi KC, Cho BJ. Thin-film thermoelectric module for power generator applications using a screen-printing method. J Electron Mater 2011;40:615.
[16] Budak S, Smith C, Muntele C, Chhay B, Herdary K, Johnson RB, et al. Thermoelectric properties of SiO_2/SiO_2+ CoSb multi-nanolayered thin films modified by MeV Si ions. J Intell Mater Syst Struct 2012;24:1350.
[17] Madan D, Wang Z, Chen A, Wright PK, Evans JW. High-performance dispenser printed MA P-type Bi(0.5)Sb(1.5)Te(3) flexible thermoelectric generators for powering wireless sensor networks. ACS Appl Mater Interfaces 2013;5:11872.
[18] Wüsten J, Potje-Kamloth K. Organic thermogenerators for energy autarkic systems on flexible substrates. J Phys D Appl Phys 2008;41:135113.
[19] Fan P, Zheng Z-H, Cai Z-K, Chen T-B, Liu P-J, Cai X-M, et al. The high performance of a thin film thermoelectric generator with heat flow running parallel to film surface. Appl Phys Lett 2013;102:033904.
[20] Bubnova O, Crispin X. Towards polymer-based organic thermoelectric generators. Energy Environ Sci 2012;5:9345.
[21] Itoigawa K, Ueno H, Shiozaki M, Toriyama T, Sugiyama S. Fabrication of flexible thermopile generator. J Micromech Microeng 2005;15:S233.
[22] Kim H, Park S-G, Jung B, Hwang J, Kim W. New device architecture of a thermoelectric energy conversion for recovering low-quality heat. Appl Phys A 2013;114:1201.
[23] Francioso L, De Pascali C, Siciliano P, De Risi A, D'Amico S, Veri C et al. Thin film technology flexible thermoelectric generator and dedicated ASIC for energy harvesting applications. In: 5th IEEE Int Work Adv Sensors Interfaces IWASI 104; 2013.
[24] Shelby MD, Clear S. Self-corrugating laminates and methods of making them, US Pat. App. 13/965,288, March 27, 2014.
[25] Yadav A, Pipe KP, Shtein M. Fiber-based flexible thermoelectric power generator. J Power Sources 2008;175:909.
[26] Gergen B, Nienhaus H, Weinberg WH, McFarland EM. Morphological investigation of ultrathin Ag and Ti films grown on hydrogen terminated Si (111). J Vac Sci Technol, B 2000;18:2401.
[27] Maréchal N. Characterization of silver films deposited by radio frequency magnetron sputtering. J Vac Sci Technol, A 1994;12:707.
[28] Gray D. American institute of physics handbook. 3rd ed. McGraw-Hill; 1982.
[29] Paddock CA, Eesley GL. Transient thermoreflectance from thin metal films. J Appl Phys 1986;60:285.
[30] Logeeswaran VJ, Kobayashi NP, Islam MS, Wu W, Chaturvedi P, Fang NX, et al. Ultrasmooth silver thin films deposited with a germanium nucleation layer. Nano Lett 2009;9:178.
[31] Parker RL, Krinsky A. Electrical resistance-strain characteristics of thin evaporated metal films. J Appl Phys 1963;34:2700.
[32] Antonova E, Looman D. Finite elements for thermoelectric device analysis in ANSYS. Int Conf Thermoelect 2005;200.
[33] Owoyele O, Ferguson S, O'Connor BT. Performance analysis of a thermoelectric cooler with a corrugated architecture. Appl Energy 2015;147:184.
[34] Rowe D, Min G. Evaluation of thermoelectric modules for power generation. J Power Sources 1998;73:193.
[35] Lee S, Song S, Au V, Moran K. Constriction/spreading resistance model for electronics packaging. Proc ASME/JSME Therm Eng Conf 1995;4:199.
[36] Song S, Lee S, Au V. Closed-form equation for thermal constriction/spreading resistances with variable resistance boundary condition. In: Proc IEPS Conf Atlanta GA, vol. 4; 1994. p. 111.
[37] Incropera FP, DeWitt DP. Introduction to heat transfer. 6th ed. Wiley; 2011.
[38] Shiozaki M, Sugiyama S, Watanabe N, Ueno H, Itoigawa K. Flexible thin-film BiTe thermopile for room temperature power generation. In: 19th IEEE international conference on micro electro mechanical systems, Istanbul; 2006.

ID	Title	Pages
771750	Heat shrink formation of a corrugated thin film thermoelectric generator	7